Çukurova Üniversitesi Mühendislik Fakültesi Dergisi, 36(4), ss. 979-987, Aralık 2021
Cukurova University Journal of the Faculty of Engineering, 36(4), pp. 979-987, December 2021

Performance Assessment of ZrO_2 Nanofibrous Oxygen Sensor

Özlem ERDEM YILMAZ[*1] ORCID *0000-0002-0976-2162*

[1]*Cukurova University, Adana Vocational School of Higher Education, Depart of Textile Technologies, Adana*

Geliş tarihi: 06.06.2021 Kabul tarihi: 10.12.2021

Atıf şekli/ How to cite: YILMAZ, Ö.E., (2021). ZrO_2 Nanolif Oksijen Sensörünün Performans Değerlendirmesi. Çukurova Üniversitesi, Mühendislik Fakültesi Dergisi, 36(4), 979-987.

Abstract

An alternative oxygen sensor to conventional ZrO_2 based automotive oxygen sensors (COS) was successfully manufactured. ZrO_2 nanoparticles were used as base material and nanofibers were fabricated via electrospinning using polyvinyl alcohol and ZrO_2 solution (ZrO_2+PVOH) to obtain active surface of the sensor where the engine exhaust gas interacts and chemisorption reactions take place prior to calcination process of nanofibers at 700 ^oC. Thanks to operating temperature control and high surface/volume ratio of nanofibrous structure, the ZrO_2+PVOH nanofibrous sensor demonstrated similar performance with COS under increasing exhaust gas percentage (until 50-60%) along with increasing operating temperature conditions. For ZrO_2+PVOH nanofibrous sensor, maximum sensing performance (R_a/R_e) of 7.24 was achieved at sensor operating temperature of 700 ^oC and exhaust gas concentration of 50% whereas it was 8.11 for EOS under same conditions. The ZrO_2+PVOH nanofibrous sensor performed acceptable performance throughout wider operating temperature range (270-900 ^oC) compared to conventional COS. Though an average of 15% reduction in sensing performance was observed for ZrO_2+PVOH nanofibrous sensor, the promising results of this alternative oxygen sensor will be a good guide for more comprehensive future works focusing on oxygen sensors with very rapid response-recovery time and light-off capability.

Keywords: Oxygen sensor, Nanofiber, Electrospinning, ZrO_2 nanoparticles, Exhaust gas

ZrO_2 Nanolif Oksijen Sensörünün Performans Değerlendirmesi

Öz

ZrO_2 tabanlı geleneksel otomotiv oksijen sensörlerine (GOS) alternatif bir oksijen sensörü başarıyla üretilmiştir. Egzoz gazlarının temas edeceği ve kimyasal reaksiyonların başlayacağı sensör aktif yüzeyini oluşturmak için, polivinil alkol ve ZrO_2'den oluşan çözelti kullanılarak (ZrO_2+PVOH) elektroeğirme yöntemiyle nanolifler elde edilmiş ve sonrasında bu lifler 700 ^oC sıcaklıkta kalsinasyon işlemine tabi tutulmuştur. İşlem sıcaklığının hassas kontrolü ve nanolif yapıların yüksek yüzey/hacim oranları sayesinde, artan egzoz gaz konsantrasyonları (%50-60'a kadar) ve yüksek çalışma sıcaklığı şartları altında, ZrO_2+PVOH nanolif sensörün GOS'a yakın ölçüm performansı gösterdiği tespit edilmiştir.

[*]Sorumlu (Corresponding author) yazar: Özlem ERDEM YILMAZ, *ozlemerdem@cu.edu.tr*

ZrO_2+PVOH nanolif sensörün 700 ^oC çalışma sıcaklığı ve %50 egzoz gaz konsantrasyonunda maksimum algılama performansı (R_a/R_e) olan 7,24'ü gösterdiği, aynı şartlar altında geleneksel oksijen sensörü için ise bu değerin 8,11 olduğu tespit edilmiştir. Nanolif sensörün geniş bir egzoz gaz sıcaklık aralığında (270-900 ^oC), kabul edilebilir algılama sonuçları gösterdiği gözlemlenmiştir. Elde edilen performans değeri, GOS'a kıyasla ortalama %15 az olsa da, bu nanolif sensör, gelecekte üretilecek daha kısa cevap-toparlanma süresine sahip ve hassas ölçüm yapabilen oksijen sensörleri için umut vadetmektedir.

Anahtar Kelimeler: Oksijen sensörü, Nanolif, Elektroeğirme, ZrO_2 nanopartikül, Egzoz gazı

1. INTRODUCTION

For many years, sensors have been irrevocable thanks to their wide usage area such as sensing physical measures, detecting hazardous and explosive gases for health and environmental concerns as studied by many researchers: Mun et.al. manufactured resistive-type lanthanum ferrite oxygen sensor based on nanoparticle-assimilated nanofiber architecture composing functional powders by sol-gel and electrospinning methods. The results demonstrate that powder formed using mixing of two methods performed the highest response time compared to that of sol-gel method. [1]. Li et.al. carried out a review study focusing on gas sensors based on semiconducting metaloxide nanostructures (SMONs) with various mechanisms including nanoparticles, nanowires, nanosheets, nanorods, etc. The research depicts that in some applications surface modification may be needed for nanoparticle based gas sensors for high sensitivity and metal ion doped SMONs are capable of adsorbing high amount of oxygen molecules due to increased number of active sites and more defects on the surfaces [2]. An experimental study on NH_3 gas sensors has been conducted by Hu et.al. [3] that is related to chemically reduced graphene oxide (rGO) based gas sensors. The promising results offer that the sensor response time is 1.4 times faster than that of the conventional NH_3 sensors. Another study on detection of volatile organic compounds (VOCs) demonstrates that $Ti_3C_2T_x$ MXene gas sensors performs quite effectiveness sensing 50–100 ppb for VOC gases at room temperature surpassing the best sensors known [4]. More related topics including detection of hazardous gases, physical measures and precautions taken against environmental and health issues can be found elsewhere [5-10]. Among these, metal oxide semiconductor sensors are renowned for their high precision in gas detection under high temperature conditions [11-14]. Oxygen sensors are to be utilized in variety of fields such as fire prevention systems [15], blood gas monitoring [16] and oxygen concentrators [17]. Likewise, automotive industry has been utilizing sensors as "sense organs" in transportation vehicles i.e. detection of pressure and temperature of intake air, motion detection (crank, detonation, ABS, etc.), impact (airbag sensors), fuel flowrate, altitude, park assistance, steering angle, etc. [18-22].

Sensing mechanism of an oxygen sensor depends on the voltage (Nernst voltage) generated by a ZrO_2 electrochemical cell. At high temperatures above 600 ^oC, oxygen ions form due to dissociation of ZrO_2 making it a solid electrolyte for oxygen. As DC current flows through a ZrO_2 disc coated with porous electrodes, oxygen ions from the atmosphere commence to be transported on the disc and an amount of oxygen at the anode is liberated proportional to the electrical charge (Figure 1) [23-26].

Although these solid-state electrochemical oxygen sensors have been well-known and have undergone development processes, they have considerable amount of drawbacks including low sensitivity to fluctuations of oxygen partial pressure and low diffusion rate of oxygen at the active layer of the sensor impairing high sensitivity [1,27,28]. A rational solution to this drawback is to present a chemical sensor comprised of metal oxide doped nanofibers fabricated via electrospinning process. The gas detection of these conductometric sensors are based on the very rapid electrical resistance

change of the surface exposed to the target gas thanks to their large SVR [1,29-31].

Electrospinning technique has always been in the radar of researchers due to its versatility, cost-effectiveness, high efficacy and simplicity in terms of nanofibrous natural and synthetic polymer fabrication. Briefly, electrospinning deals with electrostatic forces to form fiber in submicron range. Electric field, distance between feeding unit and collector, feeding rate are influential on morphology and diameter of the nanofibers in electrospinning process [32-36]. Furthermore, electrospinning is a good way of fabricating thin film layers and in chemical sensors, thin film production for sensor active surface provides considerable amount of increase in sensing efficiency since gas sensing performance is associated with active surface electrical conductivity [37-39].

This study aims to provide oxygen sensing performance evaluation of a manufactured ZrO_2 doped PVOH nanofibrous sensor under various exhaust gas fractions and sensor working temperatures in terms of sensing effectiveness considering designated engine working parameters and make a comparison to engine oxygen sensor (EOS). Nonetheless, electrospun nanofibers underwent heat-treatment process (calcination) to increase the sensing effectiveness. The morphology, chemical composition and characterization of the ZrO_2 nanoparticles and fabricated nanofibers were also presented.

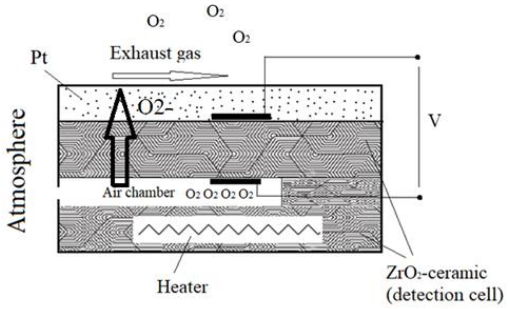

Figure 1. Schematic of a narrow-band conventional oxygen sensor [23]

2. MATERIALS & METHOD

2.1. Electrospinning Process

To prepare a homogenous polymeric solution, polyvinyl alcohol (PVOH, $M_w \approx 125000$, 88% hydrolyzed) in weight ratio of 5% was mixed with distilled water to conduct dissolution process and the mixture was maintained at 120 ^oC for 30 min. In the subsequent stage, 0.5 g (2.5%) of ZrO_2 nanoparticle powder (<100 nm, 99.5% purity, Sigma-Aldrich, Inc.) was incorporated in the PVOH solution and ultrasonicated for 5 h to impede probable precipitations and no agglomeration was observed even after 12 h of polymeric solution preparation. The data relating physical measures of the solution such as viscosity (375 cP), electrical conductivity (3.59 mS/cm) and surface tension (40 mN/m) were collected in triplicate and averaged at a mean temperature of 25 ^oC. ZrO_2 nanoparticle powder weight above as-mentioned value induced clogging in some parts of the nozzle hampering fluent electrospinning process.

Injection of the polymeric solution (PVOH+ZrO_2, injection rate of 0.1 mL/h) was carried out via a 10 mL syringe with 20-gauge nozzle towards the collector (24 cm away from the nozzle) covered with aluminum foil on which the fabricated nanofibers form a web layer at a potential difference of 22.5 kV (AC). The nanofibers were firstly transferred to microscopic thin mica and subsequent to calcination process, the nanofibers

were blended with pure water in a weight ratio of 100:20 to form a paste to coat inner and outer side of the ceramic tube [40]. The experiments were conducted at relative humidity of 45-52% and temperature of 24-28 ^{o}C (Figure 2).

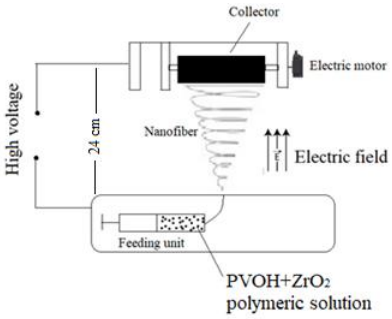

Figure 2. Illustration of the electrospinning technique

2.2. Calcination Process (Nanofiber Heat Pre-treatment)

Subsequent to electrospinning, the nanofiber layers underwent calcination (annealing) process at about 700 ^{o}C in a furnace to eliminate impurities within the nanofibers to increase the sensing performance. The calcined as-spun fibers were wrapped onto the outer (target gas side) and inner surface (reference air side) of the ceramic tube to form the active reaction surfaces (Figure 3).

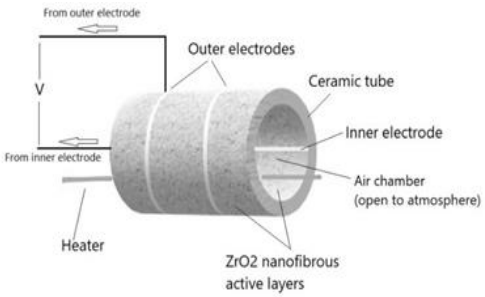

Figure 3. Illustration of the nanofibrous sensor

2.3. Characterization of the Electrospun Fibers

As-spun nanofibers were firstly gold-coated in vacuum ambient before SEM-EDX analyses to observe the structure and morphology. Subsequently, SEM images of the nanofibers were taken at 200000x magnification and in 500 nm scale. Characteristic FT-IR peaks were also analyzed to investigate fibers' structural behaviors.

2.4. Experimental Set-up

The ceramic tube with interdigitated electrodes and covered with calcined as-spun fibers was installed in a well-sealed steel chamber. The exhaust gas was sent to the chamber from an inline 4-cylinder, 3.9 liters, direct injection, turbocharged diesel test engine with maximum power of 100 kW @2900 rpm and maximum torque of 370 Nm @1600 rpm. The test engine comprises of a downpipe exhaust system (no catalytic converter, EGR, DPF, AdBlue system, etc.) with an electronically controllable valve (ECV) installed to adjust exhaust gas flow rate (Figure 4). Before each measurement, the test engine was run for a while so as to reach engine coolant regime temperature (about 70 ^{o}C) and all measurement data were collected under the engine working condition of 1750 rpm without engine load to acquire similar exhaust gas temperature of about 600-700 ^{o}C (denoted by "T" in the schematic of the set-up) for each experimental trial. Upon exposure of exhaust gas, a voltage (Nernst voltage) was generated due to the partial pressure difference of the oxygen in the air chamber (inner side) and exhaust gas (outer side) thanks to the electrolytic transporter behavior of ZrO_2 doped nanofibrous surface until a stable level was reached. This voltage informs about the surface electrical resistance (read from the multimeter) and defines response of the sensor (R_e). The outer surface of ZrO_2 doped PVOH nanofibrous sensor was exposed to the atmosphere after each test until procuring 90% change in resistance (R_a) which is also known as "recovery" of the sensor [10,29,41]. Thus, R_a/R_e was considered as the sensor detection performance throughout the study. Sensor detection performance was observed by varying sensor working temperature (from the sensor heater) and exhaust gas percentage introduced into the steel chamber through the ECV.

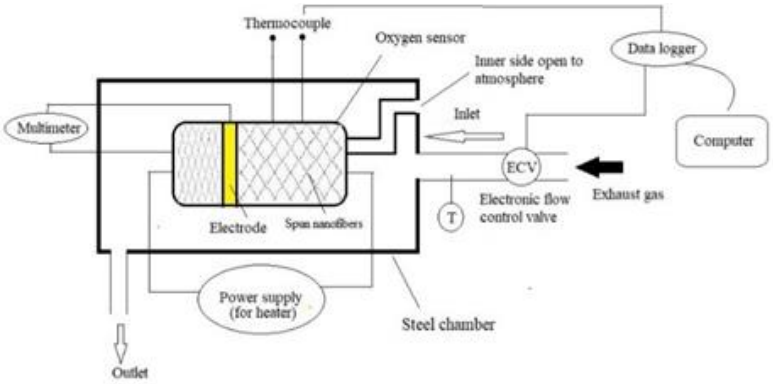

Figure 4. Illustration of the experimental set-up

3. RESULTS AND DISCUSSION

3.1. Nanofiber Characterization

Figure 5a and Figure 5b demonstrate the uniform and well-dispersed nanofiber structures of the undoped PVOH and ZrO_2 doped PVOH (polymeric solutions processed under electrostatic forces. It was observed that ZrO_2 doped PVOH nanofibers have smaller average diameters (73±8 nm) than those of the undoped PVOH nanofibers (110±12 nm). This is attributed to ionization of the solution due to the amount of metal compound providing higher electrostatic forces exerted on the polymer jet (increased whipping instability level) in the electrospinning process, thus, thinner fibers [10,42]. To the SEM image in Figure 5c, metaloxide in the ZrO_2 doped PVOH nanofibers calcined at 700 ^oC is clearly observed in bead form and nanofibers have high endurance against high temperatures (e.g. high exhaust gas temperatures). It is also seen in the EDX graph that the chemical composition of the structure decomposes from impurities at high temperatures in the calcination process [10]. Aluminum peaks are due to accumulation of the whipped fibers onto the aluminum foil and the rest of the elements support the structure of the fabricated nanofibers (Figure 5b).

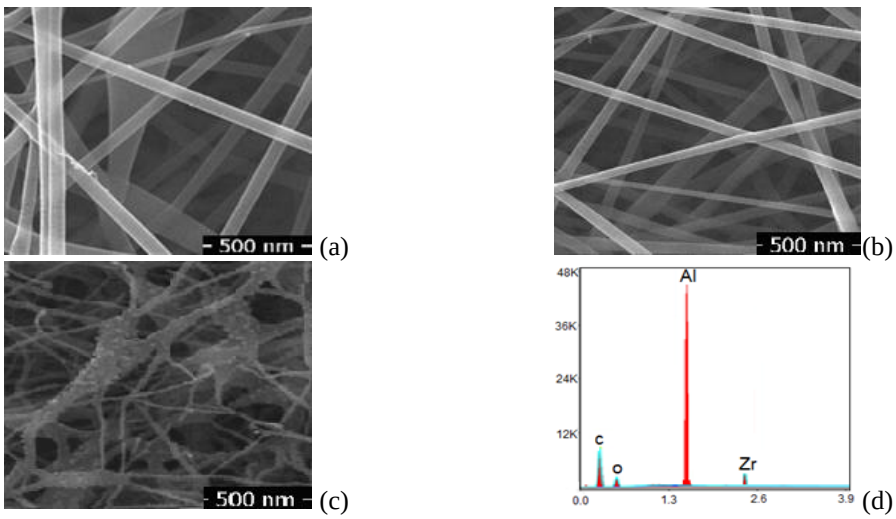

Figure 5. SEM images of the: (a) PVOH; (b) ZrO_2 doped PVOH; (c) ZrO_2 doped PVOH calcined at 700 ^oC; (d) EDX analysis of ZrO_2 doped PVOH

FT-IR spectrums (Figure 6) show that O-H and C-H peaks of PVOH are wide and flat at 3400 cm^{-1} and 2900 cm^{-1}, respectively [43]. In general, minimal shifts in PVOH may be observed in case the polymeric solution contains ZrO_2 metal oxide. Each metal has peculiar peaks in FTIR fingerprint region and it is 640 cm^{-1} for ZrO_2. A band around 1500 cm^{-1} is ascribed to Zr-O vibrations of t-ZrO_2 [44].

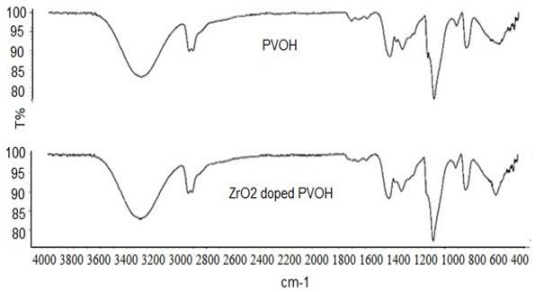

Figure 6. FT-IR spectrums of PVOH and ZrO_2 doped PVOH

3.2. Sensing Mechanism

Anion (oxygen) ion vacancies provide conduction of oxygen ions through Zr^{+4} ions. Due to almost zero electrical conductivity of stabilized zirconia at low temperatures, these sensors are to operate at minimum of 500 ^oC for applications. The platinum catalyst coats the inner and outer surfaces of the sensor to promote the electrochemical reactions as shown in Equations (1) and (2) (see Figure 1) [45]:

$$O_2 + 4e^- \rightarrow 2O^{2-} \text{ (air chamber)} \quad (1)$$

$$2O^{2-} \rightarrow O_2 + 4e^- \text{ (exhaust gas side)} \quad (2)$$

3.3. Sensing Performance

The working temperature of a zirconia oxygen sensor is a paramount parameter for AFR adjustment. In general, automotive zirconia oxygen sensors remain inactive during a time period after the cold start of the engine which is defined as "light-off capability". Within this inactive time period (average of 15 s), the sensor does not operate making a drawback in terms of meeting emission standards especially for engine cold working conditions [26]. Figure 7 presents the variation of the sensing performance of the sensor manufactured using nanofibers calcined at 700 ^oC with respect to working temperature of the sensor at constant exhaust gas percentage of 50%, exhaust temperature of 600-700 ^oC and engine speed of 1750 rpm. The ZrO_2 doped PVOH nanofibrous sensor exhibits negligible Ra/Re values (no response) until about 270 ^oC. As the temperature continues to rise, chemisorption reactions commence to accelerate and electron loss from the active surface (outer surface) provides a gradual reduction in surface electrical resistance (higher R_a/R_e). This phenomenon perpetuates until the surface comes to saturation (no more reaction between the active surface and the oxygen molecules within the exhaust gas). However, it is clearly seen from the Figure 7 that current zirconia oxygen sensor (EOS) responds beginning from 310 ^oC of operating temperature which depicts that the ZrO_2 doped PVOH nanofibrous sensor performs an effective operation in wider time period thanks to its larger SVR.

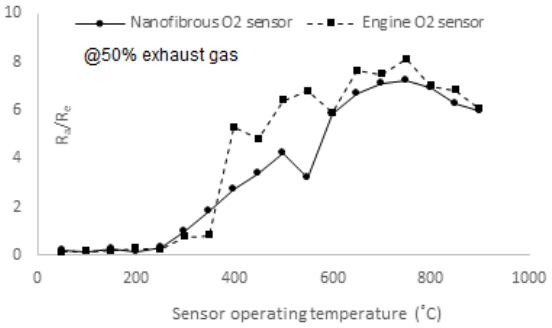

Figure 7. Sensing performance vs. sensor operating temperature

The variation of the sensors' performances versus exhaust gas percentage under constant operating temperature is shown in Figure 8. The sensor working temperature was maintained at 750 ^oC since the best performances were obtained at about this temperature value for both sensors in the former stage of the study. The increment in exhaust gas sent to the ZrO_2 doped PVOH nanofibrous sensor yields more oxygen take place in the chemical reaction, that is, more electron loss of the active surface and lower electrical resistance

(lower R_e). Reduction in electrical resistance results in higher sensing performance and reaches a stable value at about exhaust gas percentage of 50% showing that no more oxygen in the exhaust gas reacts with the ZrO_2 doped PVOH nanofibrous sensor due to saturation.

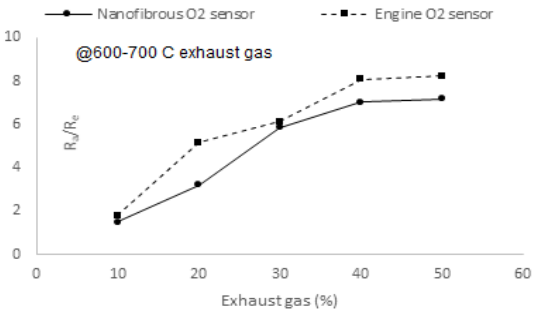

Figure 8. Sensing performance vs. exhaust gas percentage

4. CONCLUSIONS

An effective sensor has been designed and manufactured thanks to ZrO_2 doped nanofibers with high SVR. Increment of active surface area provides more interaction of exhaust gases with the sensor surface and higher effectiveness time period. The nanofibers wrapped onto the ceramic tube were fabricated via electrospinning which is a simple and cost-effective technique. The effectiveness of the ZrO_2 doped PVOH nanofibrous sensor reaches its maximum (7.24) at sensor operating temperature of about 700 ^oC which is 15% lower than that of EOS. Besides, ZrO_2 doped PVOH nanofibrous sensor depicted similar oxygen concentration measurement range (0-60%). It was shown that sensor operating temperature is paramount in oxygen sensing performance and an average performance of 3.92 was obtained at under various sensor operating temperatures. Furthermore, ZrO_2 doped PVOH nanofibrous sensor depicted high performance (average of 4.24) against increasing exhaust gas percentages. This study presents promising results in the context of oxygen detection alternatively for ICEs with high precision and can be a good guide for future works focusing on oxygen sensors with very rapid response-recovery time and light-off capability.

5. ACKNOWLEDGMENT

The author would like to thank Cukurova University, Central Research Laboratory for their technical assistance.

6. REFERENCES

1. Mun, T., Koo, J.Y., Lee, J., Kim, S.J., Umarji, G., Amalnerkar, D., Lee, W., 2020. Resistive-type Lanthanum Ferrite Oxygen Sensor Based on Nanoparticle-assimilated Nanofiber Architecture. Sensors and Actuators: B, 324, 1-12.

2. Li, Z., Li, H., Wu, Z., Wang, M., Luo, J., Torun, H., Hu, P., Yang, C., Grundmann, M., Liu, X., Fu, Y., 2019. Advances in Designs and Mechanisms of Semiconducting Metal Oxide Nanostructures for High-Precision Gas Sensors Operated at Room Temperature. Materials Horizon, 6, 470-506.

3. Hu, N., Yang, Z., Wang, Y., Zhang, L., Wang, Y., Huang, X., Wei, H., Wei, L., Zhang, Y., 2014. Ultrafast and Sensitive Room Temperature NH_3 Gas Sensors Based on Chemically Reduced Graphene Oxide. Nanotechnology, 25, 23-32.

4. Kim, S.J., Koh, H.J., Ren, C.E., Kwon, O., Maleski, K., Yeon Cho, S.S., Anasori, B., Kim, C.K., Choi, Y.K., Kim, J., Gogotsi, Y., Jung, H.T., 2018. Metallic $Ti_3C_2T_x$ MXene Gas Sensors with Ultrahigh Signal-to-Noise Ratio. ACS Nanotechnology, 12, 986-993.

5. Grassi, M., Malcovati, P., Baschirotto, A., 2005. A High-precision Wide-range front-end for Resistive Gas Sensors Arrays. Sensors and Actuators: B, 111-112, 281-285.

6. Ivanov, P., Llobet, E., Vilanova, X., Brezmes, J., Hubalek, J., Correig, X., 2004. Development of High Sensitivity Ethanol Gas Sensors Based on Pt-doped SnO_2 Surfaces. Sensors and Actuators: B, 99, 201–206.

7. Kim, Y.K., Kang, H., Kim, J.K., 2016. Directly Attached Airbag Sensor Packaging for Automobiles. Pan Pacific Microelectronics Symposium. Big Island, Hawaii, 1-3.

8. Tian, H., Shu, Y., Wang, X.F., Mohammad, M.A., Bie, Z., Xie, Q.Y., Li, C., Mi, W.T.,

Yang, Y., Ren, T.L., 2015. A Graphene-Based Resistive Pressure Sensor with Record-High Sensitivity in a Wide Pressure Range. Scientific Reports, 5, 1-6.

9. Nguyen, L.V., Warren-Smith, S.C., Ebendorff-Heidepriem, H., Monro, T.M., 2016. Interferometric High Temperature Sensor Using Suspended-core Optical Fibers. Optics Express, 24, 8967-8971.

10. Yilmaz, O.E., Erdem, R., 2020. Evaluating Hydrogen Detection Performance of an Electrospun $CuZnFe_2O_4$ Nanofiber Sensor. International Journal of Hydrogen Energy, 45, 26402-26412.

11. Seo, Y., Memon, M.U., Lim, S., 2016. Microfluidic Eighth-mode Substrate-integrated-waveguide Antenna for Compact Ethanol Chemical Sensor Application. IEEE Transactions on Antennas and Propagation, 64, 3218-3222.

12. Aslani, A., Oroojpour, V., 2011. CO Gas Sensing of CuO Nanostructures Synthesized by an Assisted Solvothermal Wet Chemical Route. Physica B: Condensed Matter, 406, 144-149.

13. Nagarajan, V., Chandiramouli, R., 2019. Detection of Trace Level of Hazardous Phosgene Gas on Antimonene Nanotube Based on First-principles Method. Journal of Molecular Graphics and Modelling, 88, 32-40.

14. Van Hoang, N., Hung, C.M., Hoa, N.D., Van Duy, N., Van Hieu, N., 2018. Facile On-chip Electrospinning of $ZnFe_2O_4$ Nanofiber Sensors with Excellent Sensing Performance to H_2S Down ppb Level. Journal of Hazardous Materials, 360, 6-16.

15. Bhattacharjee, S., Roy, P., Ghosh, S., Misra, S., Obaidat, M.S., 2012. Wireless Sensor Network-based Fire Detection, Alarming, Monitoring and Prevention System for Bord-and-Pillar Coal Mines. Journal of System and Softwares, 85, 571-581.

16. Iguchi, S., Mitsubayashi, K., Uehara, T., Ogawa, M., 2005. A Wearable Oxygen Sensor for Transcutaneous Blood Gas Monitoring at The Conjunctiva. Sensors and Actuators: B, 108, 733–737.

17. Chatburn, R.L., Williams, T.J., 2010. Performance Comparison of 4 Portable Oxygen Concentrators. Respiratory Care, 55, 433-442.

18. Fleming, W.J., 2001. Overview of Automotive Sensors. IEEE Sensors Journal, 1, 296-308.

19. Grace, R.H., 2001. Application Opportunities of MEMS/MST in the Automotive Market: The Great Migration from Electromechanical and Discrete Solutions, Springer, Berlin, 1-16.

20. Hoffman, D., Rizzo, M., 1998. Chevrolet C5 Corvette Vehicle Dynamic Control System. SAE Technical Paper, 980233, 1-8.

21. Eddy, D., Sparks, D., 1998. Application of MEMS Technology in Automotive Sensors and Actuators. Proceeding IEEE, 86, 1747–1755.

22. Frank, R., 1998. Future Sensing in Vehicle Applications. Sensors and Transducers, 25, 36-45.

23. Litzelman, S.J., Rothschild, A., Tuller, H.L., 2005. The Electrical Properties and Stability of $SrTi_{0.65}Fe_{0.35}O_3{-}\delta$ thin Films for Automotive Oxygen Sensor Applications. Sensors and Actuators: B, 108, 231–237.

24. SST Sensing: Zirconium Dioxide (ZrO_2) Oxygen Sensor Operating Principle Guide. https://sstsensing.com/wpcontent/uploads/2016/05/AN0043_rev5_Zirconia-Sensor Operating-Principle and Construction-Guide.pdf 2017. Accessed 10 February 2021

25. Ritter, T., Hagen, G., Lattus, J., Moos, R., 2018. Solid State Mixed-potential Sensors as Direct Conversion Sensors for Automotive Catalysts. Sensors and Actuators: B, 255, 3025–3032.

26. Riegel, J., Neumann, H., Wiedenmann, H.M., 2002. Exhaust Gas Sensors for Automotive Emission Control. Solid State Ionics, 152–153, 783– 800.

27. Bektas, M., Stocker, T., Mergner, A., Hagen, G., Moos, R., 2018. Combined Resistive and Thermoelectric Oxygen Sensor with Almost Temperature-independent Characteristics. Journal of Sensors and Sensor Systems, 7, 289–297.

28. Wiedenmann, H.M., Hotzel, G., Neumann, H., Riegel, J., Stanglmeier, F., Weyl, H., 1999. Exhaust gas sensors, Automotive Electronics Handbook. McGraw-Hill, New York.

29. Xu, X., Sun, J., Zhang, H., Wang, Z., Dong, B., Jiang, T., Wang, W., Li, Z., Wang, C., 2011. Effects of Al Doping on SnO_2 Nanofibers in

Hydrogen Sensor. Sensors and Actuators: B, 160, 858-863.

30. Huang, J., Wan, Q., 2009. Gas Sensors Based on Semiconducting Metal Oxide One-dimensional Nanostructures. Sensors, 9, 9903-9924.

31. Comini, E., Faglia, G., Sberveglieri, G., 2002. Stable and Highly Sensitive Gas Sensors Based on Semiconducting Oxide Nanobelts. Applied Physics Letters, 81, 1869-1871.

32. Erdem, R., Yuksek, M., Sancak, E., Atak, O., Erginer, M., Kabasakal, L., Beyit, A., 2017. Electrospinning of Single and Multilayered Scaffolds for Tissue Engineering Applications. Journal of Textile Institute, 108, 935-946.

33. Budun, S., Isgoren, E., Erdem, R,. Yuksek, M., 2015. Morphological and Mechanical Analysis of Electrospun Shape Memory Polymer Fibers. Applied Surface Science, 380, 294–300.

34. Erdem, R., Akalin, M., 2015. Characterization and Evaluation of Antimicrobial Properties of Electrospun Chitosan/Polyethylene Oxide Based Nanofibrous Scaffolds (with/without Nanosilver). Journal of Industrial Textiles, 44, 553–571.

35. Erdem, R,. Ilhan, M., Sancak, E., 2015. Analysis of EMSE and Mechanical Properties of Sputter Coated Electrospun Nanofibers. Applied Surface Science, 380, 326–330.

36. Erdem, R., Usta, I., Akalin, M., Atak, O., Yuksek, M., Pars, A., 2015. The Impact of Solvent Type and Mixing Ratios of Solvents on The Properties of Polyurethane Based Electrospun Nanofibers. Applied Surface Science, 334, 227–230.

37. Shahabuddin, M., Umar, A., Tomar, M., Gupta, V., 2017. Custom Designed Metal Anchored SnO_2 Sensor for H_2 Detection. International Journal of Hydrogen Energy, 42, 4597-4609.

38. Yamazo, N., 1991. New Approaches for Improving Semiconductor Gas Sensors. Sensors and Actuators: B, 5, 7-19.

39. Yamazo, N., Shimano, K., 2009. New Perspectives of Gas Sensor Technology. Sensors and Actuators: B, 138, 100-107.

40. Liu, L., Li, S., Zhuang, J., Wang, L., Zhang, J., Li, H., Liu, Z., Han, Y., Jiang, X., Zhang, P., 2011. Improved Selective Acetone Sensing Properties of Co-doped ZnO Nanofibers by Electrospinning. Sensors and Actuators: B, 155, 782-788.

41. Liang, Y.X., Chen, Y.J., Wang, T.H., 2004. Low-resistance Gas Sensors Fabricated from Multiwalled Carbon Nanotubes Coated with a Thin Tin Oxide Layer. Applied Physics Letters, 85, 666-668.

42. Sancak, E., Ozen, M.S., Erdem, R., Yilmaz, A. C., Yuksek, M., Soin, T., Shah, T., 2018. PA6/Silver Blends: Investigation of Mechanical and Electromagnetic Shielding Behavior of Electrospun Nanofibers. Tekstil ve Konfeksiyon, 28, 229-235.

43. Kharazmi, A., Faraji, N., Mat Hussin, R., Saion, E., Yunus, W.M.M., Behzad, K., 2015. Structural, Optical, Opto-Thermal and Thermal Properties of Zns–PVA Nanofluids Synthesized Through Aradiolytic Approach. Beilstein Journal of Nanotechnology, 6, 529–536.

44. Madhusudhan, H.C., Shobhadevi, S.N., Nagabhushana, B.M., Chaluvaraju, B.V., Murugendrappa, M.V., Krishna, R.H., Nagabhushana, H., Radeep, N.R., 2016. Effect of Fuels on Conductivity, Dielectric and Humidity Sensing Properties of ZrO_2 Nanocrystals Prepared by Low Temperature Solution Combustion Method. Journal of Asian Ceramics Society, 4, 309-318.

45. Sjoholm, P., Ingham, D.B., Torvela, H., 2001. Gas Cleaning Technology, Industrial Ventilation Design Guidebook, Elsevier, 1197-1316.